High gain in a dual-pass rod-type fiber amplifier

Lupi, Jean François; Johansen, Mette Marie; Michieletto, Mattia; Christensen, Simon Lønborg; Lægsgaard, Jesper

Published in:
Journal of the Optical Society of America B: Optical Physics

Link to article, DOI:
10.1364/JOSAB.381433

Publication date:
2020

Document Version
Publisher's PDF, also known as Version of record

Research Article Vol. 37, No. 2 / February 2020 / Journal of the Optical Society of America B 451

Journal of the Optical Society of America B

OPTICAL PHYSICS

High gain in a dual-pass rod-type fiber amplifier

JEAN-FRANÇOIS LUPI,[1] METTE MARIE JOHANSEN,[2] MATTIA MICHIELETTO,[2] SIMON LØNBORG CHRISTENSEN,[1,2] AND JESPER LÆGSGAARD[1,*]

[1]DTU Fotonik, Department of Photonics Engineering, Technical University of Denmark, 2800 Kgs. Lyngby, Denmark
[2]NKT Photonics, Blokken 84, 3460 Birkerød, Denmark
*Corresponding author: jlag@fotonik.dtu.dk

Received 24 October 2019; revised 13 December 2019; accepted 17 December 2019; posted 18 December 2019 (Doc. ID 381433); published 28 January 2020

Single-pass amplification using rod-type fibers has become a common route to pulsed laser sources around 1030 nm with high average and peak power. Average-power scaling is currently limited by the dynamic thermo-optic phenomenon of "transverse mode instability." In comparison, double-pass amplifier configurations have not been extensively studied. Recent theoretical and experimental work has shown both static and dynamic mode degradation phenomena, including an unexpected nonlinear polarization rotation effect. Here we present new results obtained with a modified setup using polarization filtering between the first and the second pass. We obtain up to 113 W output power, i.e., more than 40 dB of amplification from a single amplifier module seeded by 10 mW of 20 ps/20 MHz/1030 nm pulses. We observe excellent beam quality and polarization extinction ratio. Finally, we investigate a wide range of seed powers and report a strong increase in the static mode deformation threshold with decreasing seed power. The experimental results are corroborated by numerical simulations.

https://doi.org/10.1364/JOSAB.381433

1. INTRODUCTION

Amplifier systems using Yb-doped fiber with large cores have become a standard method to produce high-power infrared sources with high average-power levels and extreme pulse properties in terms of, e.g., duration and peak power [1–3]. The actual limitation for scaling of average power in a single-pass amplification module, despite many studies on comprehension and mitigation, remains the so-called transverse mode instability (TMI) [3–14], a low-frequency dynamic instability phenomenon. In contrast, only a few studies on the double-pass configuration at high average-power levels have appeared [15–18]. According to these publications, two instability phenomena are found to occur in dual-pass rod-type fiber amplifiers: static mode degradation (SMD) and dynamical TMI. Both are thought to consist of coupling between modes (spatial and/or polarization) through a thermo-optic nonlinear grating induced by the beating between these modes. More precisely, theoretical considerations suggest that SMD is due to scattering between co-propagating modes on thermo-optic index gratings set up by the counter-propagating modes [15]. On the other hand, TMI is commonly believed to be due to scattering between co-propagative modes and a grating set up by the same co-propagative modes [6,9,11,12]. The fundamental difference between SMD and TMI is that TMI requires a specific frequency down-shift between coupled modes, and SMD does not. Because of this down-shift, TMI must be seeded by technical or shot noise [10,19–21], whereas SMD may be seeded from the part of the signal inadvertently coupled into higher-order modes (HOMs). Because of these different origins, TMI is dynamic (0–5 kHz), while SMD is static. A more precise description of SMD can be found in recent theoretical [15] and experimental publications [17].

In the case of single-pass, the TMI threshold can be defined as the onset of a temporal fluctuation measured at the center of the beam [22] or as rapid degradation of M^2 [5]. In this case, the output power continues to increase into the unstable regime. In the particular case of dual-pass, the output power peaks and then decreases with pump power along with the gradual increase in SMD, and dynamic TMI has been found to set in as pump power is increased beyond the signal power maximum [17].

In double-pass amplifier setups, a Faraday rotator is used to turn the signal polarization 90° between the first and second passes, which means that a linearly polarized input will emerge in the orthogonal linear polarization state after the two passes, irrespective of intended or unintended birefringence in the amplifier. Input and output signals can then be separated by a polarizing beam splitter (PBS). In previous work [17], we found that the onset of SMD was characterized by an unexpected polarization change, with part of the optical power emerging from the double-pass amplifier in the polarization state rejected by the final PBS. While it is known that a linear polarization input to the LP_{11} modes of a fiber will rotate due to the vectorial

nature of the true eigenmodes, this polarization should also in principle be undone by the Faraday rotation. This is, however, not the case if light is coupled into the HOM during the passage through the amplifier, e.g., by thermo-optic mode coupling. Still, the phenomenon is somewhat unexpected, because the splitting between vectorial modes in the LP_{11} multiplet in a step-index fiber with a large core size is extremely low, and a noticeable polarization rotation would not be expected in amplifier lengths on the order of 1–2 m. Alternatively, one may speculate that the polarization change comes about in some of the optical components external to the amplifier, i.e., Faraday mirror, lenses, PBS, etc., due to deformations occurring in high-power operation. One purpose of the present work is to elucidate this question by inserting a polarization filter between the first and second passes of the amplifier, and varying the beam spot size on the feedback components to distinguish thermal or intensity-dependent effects.

A key feature of double-pass amplifiers is the possibility to obtain very high gains. Since the gain of a single-pass power amplifier is typically in the range of 10–20 dB, gains of 20–40 dB should be possible in a double-pass configuration. A gain approaching 40 dB would allow amplification from a low-power seed oscillator to ∼100 W power levels only in the double-pass stage, which makes for a simple and compact laser system with a relative low cost. Thus, it is of high interest to study the dependency of the SMD threshold on gain, and in particular, the behavior in high-gain configurations. In this paper, we investigate this question by varying the seed power over two orders of magnitude, from 10 mW to 1 W.

Remarkably, the results presented in this work show that the SMD threshold is maximal in the case of a high amplifier gain. Furthermore, it is demonstrated that the polarization rotation effect observed is in all likelihood caused by polarization rotation in the fiber itself. The addition of intermediate polarization filtering in fact appears to have decreased the SMD threshold for a given seed power compared to our previous work. These experimental findings are corroborated by theory and simulation studies.

Experimentally, we obtain up to 113 W output power, i.e., more than 40 dB of amplification when seeded with 10 mW of 20 ps/20 MHz/1030 nm pulses. We observe excellent beam quality and polarization extinction ratio (PER). TMI is observed right above this maximum power of 113 W. Seeding with higher powers is found to decrease both the maximal extractable signal power and the threshold for onset of SMD. Simulation studies indicate that this trend is related to the efficient gain suppression of HOMs in the microstructured rod amplifier used for the experiments. These findings suggest that the primary application potential for large-core double-pass amplifiers is as high-gain amplifier modules at average output power levels of ∼100 W.

The rest of this paper is structured as follows. In Section 2, the experimental setup for dual-pass amplification is described, highlighting the difference between this setup and the one used in our previous work. In Section 3, experimental results for SMD and TMI with 10 mW seed are presented, and in Section 4, results for SMD with higher seed powers are shown. Then, in Section 5, finite-element simulations of the amplifier's modal properties and simulations of static thermo-optic mode coupling for different input seed powers are presented and discussed. Section 6 summarizes our conclusions.

2. EXPERIMENTAL SETUP

Figure 1 describes the experimental setup used to perform dual-pass amplification experiments. The seed laser is a commercially available aeroPULSE laser with a mode-locked source emitting up to 10 W of 20 ps pulses at a repetition rate of 20 MHz and at a central wavelength of 1030 nm. The seed is operated at 5 W. An isolator protects the seed laser, and a telescope is used to filter any HOM content (in forward and backward propagation). A first PBS is used to collect and analyze the backward-propagating power. The seed is fully transmitted by this PBS. Then the seed is injected into a rod-type fiber by two mirrors, a half-wave plate, a PBS, a second half-wave plate, a long-pass dichroic mirror, and a 60 mm lens. The two mirrors and the lens are used for the alignment procedure, and the long-pass dichroic mirror is used in order to remove non-absorbed pump power. The second PBS is also used as the main output, the first half-wave plate sets the seed transmission through the second PBS, and the second half-wave plate is used to minimize backward-propagating power. The rod-type fiber is an aeroGAIN-ROD-PM85 (NKT Photonics) based on distributed mode filter design [23]; it has a core diameter of 85 μm, a pump cladding of 260 μm with 0.6 NA, and a length of 80 cm. Both ends are protected by anti-reflection-coated end caps. Thermal management is provided by water-cooling along the rod. After the rod, a 20 mm lens is used to collimate the output and focus the pump light, while a short-pass dichroic mirror separates the pump and the signal. Then two lenses (−25 mm and +50 mm), a Faraday rotator, a half-wave plate, a third PBS, a −50 mm lens, and a concave mirror provide the feedback. The Faraday rotator turns the polarization by $2 \times 45^\circ$ for all polarizations, and the half-wave plate and the third PBS select one of these polarizations. The backward-propagating signal is re-amplified a second time by the rod and finally separated by the first PBS, the second PBS, and the isolator's outputs.

There are two outputs: the main and the discarded, respectively, from the second and the first PBS. The light rejected by the isolator is not analyzed. Power and beam profile measurements are performed on the two outputs. A 250 W power meter (Ophir-FL250A) is used on the main output, and a 3 W power meter (Ophir-PD300R-3W) is used on the discard output. Imaging of the rod output is performed with a camera (Spiricon-SP300). The measurements presented are performed with seed power spanning from 10 to 1000 mW (after the second PBS), a repetition rate of 20 MHz, and pump power between 0 and 300 W.

The differences in this setup compared to that used in [17] are as follows. A telescope is used to protect the seed. The non-polarizing beamsplitter (N-PBS) is replaced by the first PBS. The pump source is changed. A short-pass dichroic mirror is used to separate the pump and signal on the feedback instead of a long-pass dichroic mirror, as in the previous work. The telescope on the feedback previously had −50 and +100 mm lenses, and now it has −25 and +50 mm lenses. These changes are practical, and we do not expect them to affect the results. The main difference from the previous setup is the addition

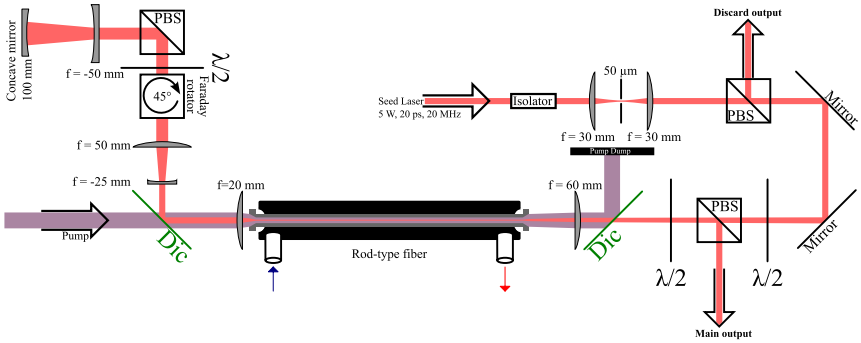

Fig. 1. Experimental setup for dual-pass amplification. PBS, polarizing beam splitter; Dic, dichroic mirror.

of a half-wave plate and a third PBS to the feedback. Finally, the feedback mirror is replaced by a convex lens and a concave mirror.

In order to investigate whether power-dependent changes in the optical feedback components affected system performance, we also performed measurements with/without the second telescope and with a plane mirror and a concave lens instead of a convex lens and a concave mirror. In these four combinations, the beam surface area changes by a factor of four on the third PBS and the Faraday rotator, and by a factor of 10,000 on the mirror. Similar results were found in these four combinations, which makes it unlikely that nonlinear effects in the feedback components play any significant role in explaining the observed system behaviors. Finally, we confirmed the results with several different rods of the same kind and observed similar results. Therefore, we can exclude any degradation such as photo-darkening.

3. RESULTS WITH LOW SEED

Figure 2 shows main and discarded powers as a function of pump power for 10 mW input seed power. The main power grows linearly with pump power up to a maximum at 113 W output for 264 W pump power. After this maximum, the output power decreases. In the meantime, the discarded power slowly increases up to 2.7 W at 264 W pump, close to maximal power, followed by a more rapid increase up to 4.5 W at 268 W pump. At threshold, the amplifier module delivers 40 dB of gain with an internal PER of 16 dB and an efficiency of 43%.

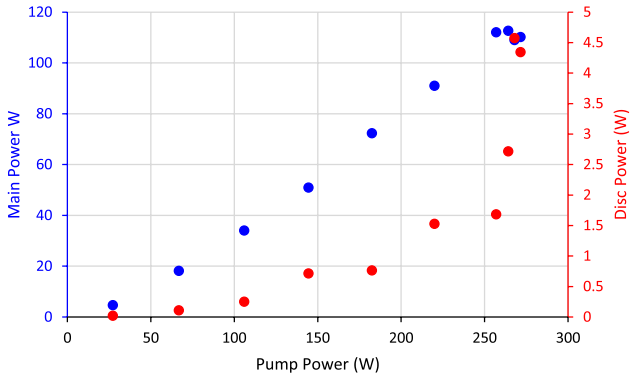

Fig. 2. Main (blue solid circle) and discarded (red solid circle) powers as function of pump power at 10 mW input seed power.

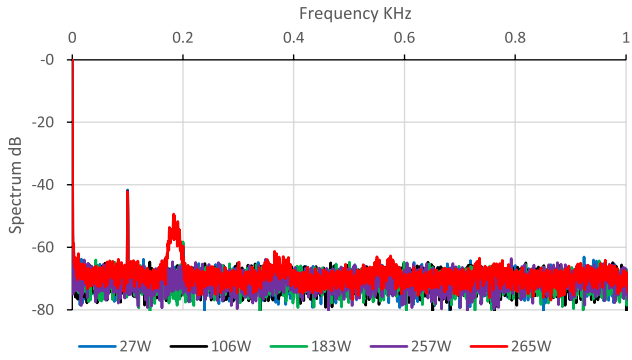

Fig. 3. Power spectra for several pump powers and 10 mW seed.

Dynamical spatial fluctuations (TMI) in single-pass amplifiers are typically quantified by measuring a time series of the power in a small part of the beam, e.g., by pinhole detection. A convenient alternative in the double-pass setup is to measure power fluctuations in the full beam on the discard output, which, as shown below, is primarily in HOMs. The time series can be Fourier transformed to obtain a spectrum of the power fluctuations. Figure 3 shows such power spectra for several values of the pump power at 10 mW seed, obtained by fast detection with a photo-diode. The spectra are plotted from 0 to 1 KHz, where the first resonances of TMI are found to occur for the dual-pass system [17]. At 257 W pump and below, there is no trace of dynamic behavior and therefore no trace of TMI. Then TMI appears at 265 W pump with a frequency "peak" at 180 Hz followed by few resonances. Measurement are performed up to 5 kHz, and we see background noise only above 1 kHz for these pump and seed powers. We note here that while the TMI observed in Fig. 3 is clearly above the noise floor of the measurements, it is still significantly below the levels commonly adopted for defining TMI thresholds in single-pass fibers. Since TMI in the double-pass amplifier is preceded by a power maximum and static beam deformations, it is not of interest to establish a more quantitative definition of TMI threshold in this case.

Figure 4 shows selected images of the main and the discarded output for different pump powers. Images (a)–(c) are the main outputs for 67, 183, and 265 W pump corresponding to 18, 72, and 112 W outputs. The main beam exhibits a nearly Gaussian shape for all pump powers. Images (d)–(f) are the discarded beam profiles for the same pump powers and 110 mW, 760 mW,

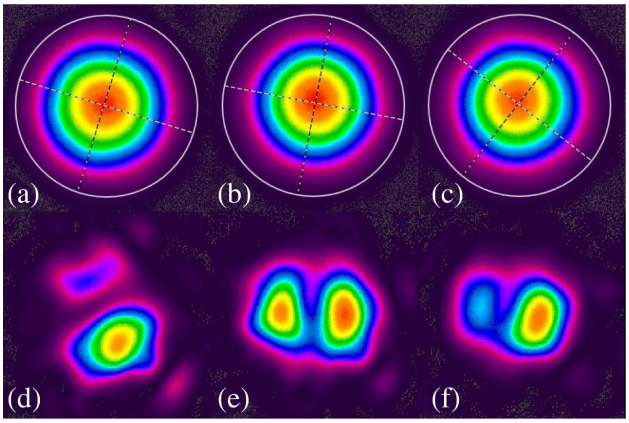

Fig. 4. Selected images of the main and discarded outputs obtained from 10 mW seed. (a) Main output 18 W from 67 W pump. (b) Main output 72 W from 183 W pump. (c) Main output 112 W from 265 W pump. (d) Discarded output 110 mW from 67 W pump. (e) Discarded output 760 mW from 183 W pump. (f) Discarded output 3 W from 265 W pump. The white circle is a 90 μm aperture. All images have the same scale.

and 3 W discarded powers, respectively. The discarded beam appears like a mixture of fundamental and LP_{11}-like modes, evidencing the presence of these two modes on the discarded polarization.

Images (a), (b), (d), and (e) are below the SMD threshold, while (c) and (f) are above threshold. At this low seed power, there is no qualitative difference in images below and above threshold except for a little "flickering" in image (f).

4. RESULTS WITH HIGHER SEED

Figure 5 shows the main power as a function of pump power for seed power spanning from 10 to 1000 mW.

For all input seed powers, the main output power increases with pump power up to a maximum, then it decreases upon further increase in pump power. This behavior corresponds to our previous observations (Fig. 2 and [17]) in which the signal power maximum was found to correlate with the onset of TMI at a magnitude noticeable in the power spectra of the discarded signal. The maximum output power depends on the input seed power—the lower the input the higher the output. The 44% efficiency is relatively low, but this is due to our pump source,

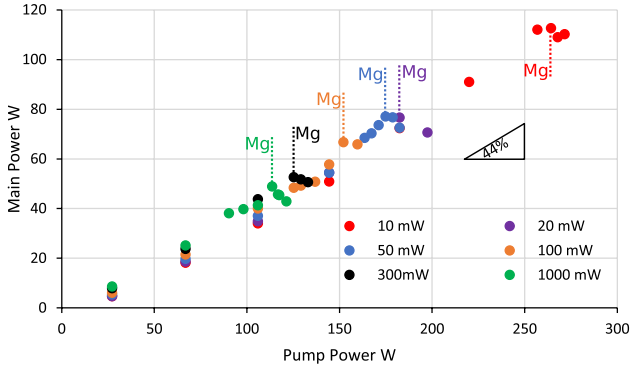

Fig. 5. Main power as function of pump power for various input powers. Maximum gain (Mg) is indicated for each seed power.

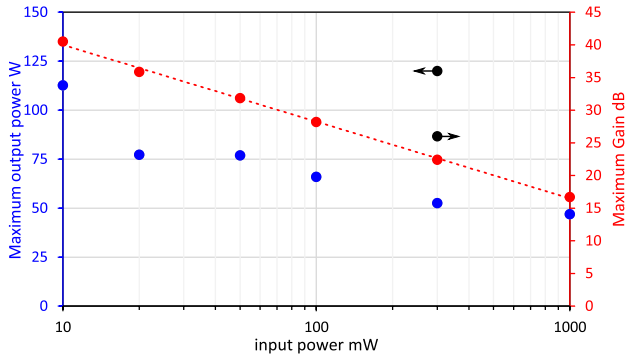

Fig. 6. Maximum power (blue solid circle) and gain (red solid circle) achievable as function of input power in lin–log scale. Dashed red line is logarithmic fit for maximum gain. Blacks dots: previous work [17].

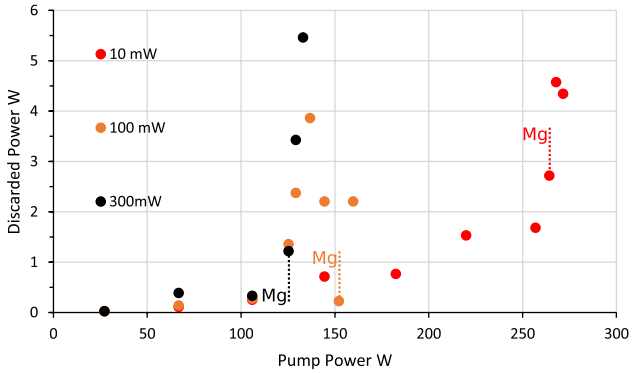

Fig. 7. Discarded power as function of pump power for various input powers. Maximum gain (Mg) is indicated for each seed power.

which is optimized for higher power, meaning that the pump wavelength is slightly detuned from the Yb^{3+} absorption peak at the power levels utilized in this work.

Figure 6 shows maximum achievable power and gain as a function of pump power for seed power spanning from 10 to 1000 mW. The two black dots correspond to our previous work on dual-pass amplification [17].

Maximum gain values are fitted with a logarithmic law. This dependency follows trivially if one assumes a constant (pump-power-limited) output power. In fact, the maximum power varies with seed power, but only by a factor of ~2.5 for a seed variation over two orders of magnitude. Therefore, the logarithmic fit is quite good. The maximum power variation is bumpy, and cannot be convincingly fitted by a simple function such as a logarithmic or power-law dependence. At this point, we do not have a quantitative theory to explain these variations. At 300 mW seed power, maximum output power is lower by a factor of 2.4 than in our previous work [17]. Since no nonlinear perturbations on the optical components in the feedback loop were established when changing the optical setup, as discussed in Section 3, this reduction factor is likely due to an increased intermodal coupling from the additional PBS.

Figure 7 shows discarded power as a function of pump power for 10 mW in red, 100 mW in orange, and 300 mW in black.

For discarded power, two different cases occur. The first one, represented by 10 and 300 mW in Fig. 7, is a soft and monotonic

increase in discarded power up to the signal power maximum where discarded power increases suddenly. This first behavior is quite similar to our previous observations [17], even if the discarded powers below the maximum are relatively low and stable compared to the exponential-like behavior in [17]. The second one is the particular case of 100 mW seed. In that case, discarded power grows before the signal power maximum is reached, up to 4 W discarded power, then falls back to ∼100 mW and finally increases again after the maximum. These different behaviors may be due to the multistable nature of the double-pass amplifier system in certain regimes, suggested by the numerical results presented in the next section as well as in [15]. An alternative explanation could be that the HOM light goes through a full polarization rotation so that the discarded power is accidentally very low at one measurement point.

5. NUMERICAL RESULTS AND DISCUSSION

A. Nonlinear Coupled-Mode Model

In single-pass TMI models, gain saturation has been found to increase the TMI threshold [24,25], so the present experimental finding of a strong threshold increase upon seed power reduction may seem surprising, since reduction in seed power also reduces gain saturation. Therefore, it is of interest to investigate whether current models of double-pass instabilities can provide some insight into the underlying mechanisms. In this section, the experimental results will be simulated using the model presented in [15]. It should be stressed from the outset that this model does not fully describe the experimental situation and cannot be expected to provide quantitatively accurate results. In particular, the model does not account for the cross-polarization couplings that are clearly observed in experiments, and it is based on a coupled-mode expansion into one LP_{01} and one LP_{11} mode calculated for a step-index fiber, whereas especially the HOM in the actual rod amplifier has a much more complex structure. Furthermore, the model does not account for thermo-optic modifications of the modal profiles, and it ignores all dynamical effects. Due to the moderate levels of power extraction, thermal mode deformations are not expected to be large, and dynamical effects are found to set in after the appearance of static deformations, so these latter caveats are maybe less important. The model does include gain saturation effects in a first-order expansion [25], and with a detailed account of the 2D spatial hole-burning profile.

To understand the results of the model, it is important to note that the double-pass problem is qualitatively different from the single-pass case. Single-pass amplification is a straightforward propagation problem, where (in the coupled-mode picture) a set of first-order differential equations connect a given input state (pump and seed powers, seed modal distribution) to a well-defined output state, possibly with random noise if temporal dynamics is considered. The double-pass amplifier, on the other hand, is more like a nonlinear boundary value problem, due to the nonlinear thermo-optic coupling between forward- and backward-propagating signals. With given values for pump power and signal amplitudes for both forward- and backward-propagating modes at the input/output end, integration of first-order nonlinear coupled mode equations can determine the corresponding amplitudes at the reflection end. However, only the forward-propagating (input) amplitudes are known. The backward-propagating (output) amplitudes must be determined to satisfy a specified relation between forward- and backward-propagating amplitudes at the reflection end. Such a problem can have several solutions for a given set of input amplitudes, and it is a non-trivial task to map out these solutions. In the calculations shown here, a Newton–Raphson steepest-descent approach was used to solve for the output amplitudes, starting from an initial guess typically obtained from a previous calculation with slightly different parameters (more details can be found in [15]). Typically, the pump power is stepped up or down, but in some cases, it is also necessary to make incremental steps in the seed power level, in particular to obtain states with significant HOM content when the seed power is low.

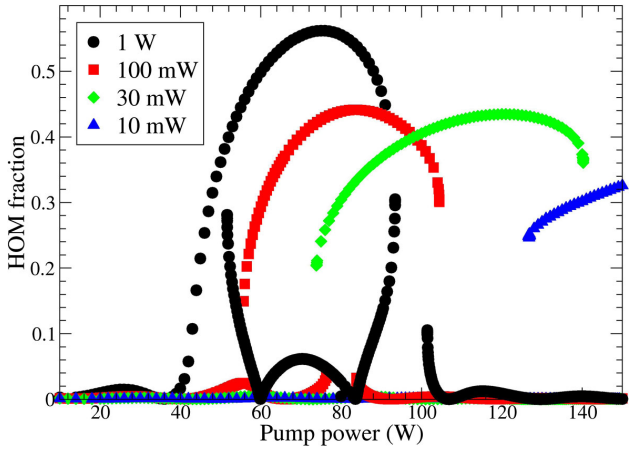

Fig. 8. Higher-order mode fractions as function of pump power for all solutions identified with seed powers of 1 W (black circles), 100 mW (red squares), 30 mW (green diamonds), and 10 mW (blue triangles).

In the simulations, a double-clad step-index fiber with a core radius of 40 μm, inner cladding radius of 130 μm, and a small-signal absorption of 300 dB/m for core pumping at 976 nm is used. The fiber length is set to 80 cm to mimic the experiments. The core V-parameter is taken to be 2.7, which gives core overlap fractions of 0.87 and 0.52 for the LP_{01} and LP_{11} modes, respectively. In a numerical model of the aeroGAIN-ROD-PM85 structure (see Section 5.B), the corresponding overlaps are 0.84 for the fundamental mode and 0.38–0.43 for the various vectorial modes in the LP_{11} multiplet. The LP_{11} overlaps are somewhat sensitive to the exact core index of the amplifier, which is hard to characterize experimentally, but most likely, gain suppression of these modes is better in the experimental rod than in the model. As will be shown, the presence of a strong gain suppression is important to understand the behavior of the SMD threshold with seed power. A 1% HOM fraction in the input signal was assumed in all calculations. Perfect reflection of both modes at the reflection end of the amplifier was assumed, as we have no immediate way of estimating reflection coupling coefficients, a simplification that may significantly impact the quantitative results obtained.

Figure 8 shows the fraction of power in the LP_{11} mode, subsequently denoted "HOM fraction," as a function of pump power for all solutions identified with four different seed power levels. At a seed level of 1 W, a continuous evolution from low to

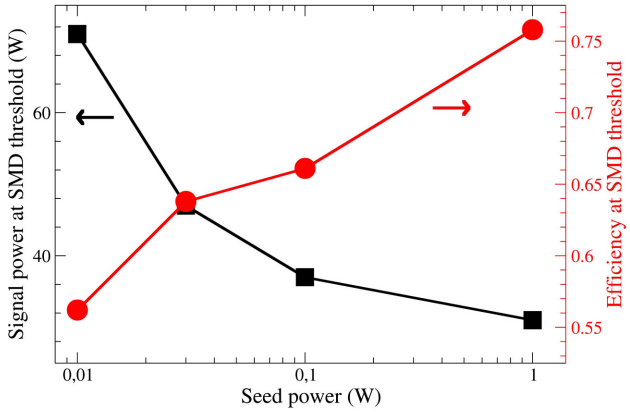

Fig. 9. Simulated LP_{01} signal power (black squares) and amplifier efficiency (red circles) at SMD threshold versus seed power.

high HOM fraction is observed as the pump power is increased, whereas at the same time, another low-HOM solution appears. However, for a seed level of 100 mW, there is a discontinuous jump between states with low and high HOM fractions. When further reducing the seed power to 30 or 10 mW, a continuous low-HOM state was found across the range of pump powers investigated, but high-HOM states could also be identified above a certain threshold, which increased with decreasing seed power. It should be noted here that we did observe bi-stable behavior experimentally, and it was particularly clear for the higher seed powers. The system can be swapped between states with widely different levels of discarded power by changing the position of the −50 mm lens.

The maximal LP_{01} signal power obtained before onset of mode deformation at a seed power of 1 W was 31 W. With increasing pump power, the total signal power kept increasing, but only due to the LP_{11} component. The appearance of a power maximum in the experiments must therefore be ascribed to polarization rotation in the LP_{11}-like modes, which drains a part of the LP_{11} power from the output port.

In Fig. 9, the power in the fundamental mode at the SMD threshold is plotted as a function of seed power. For the 1 W seed, the SMD threshold is defined by the power maximum in the LP_{01} signal mode described above. For the lower seeds, it is defined as the power in the LP_{01} mode in the solution with low HOM content at the lowest power level for which the second solution with high HOM content can be identified in the simulations. Clearly, the simulations predict a strong increase in the threshold signal power with decreasing seed power, in qualitative agreement with the experiments. It is noteworthy that the simulations reproduce the experimental trend in spite of the fact that it includes gain saturation effects that tend to pull in the opposite direction.

The downside to reducing seed power is a reduced efficiency, because the corresponding high amplifier gain necessitates a strong population inversion, and thus reduced pump absorption. The efficiency, defined as LP_{01} signal power at threshold divided by pump power is shown by the red curve in Fig. 9. In this connection, it should be noted that the pump wavelength in the simulation was fixed at the Yb absorption peak of 976 nm, i.e., the thermal drift of the pump wavelength present

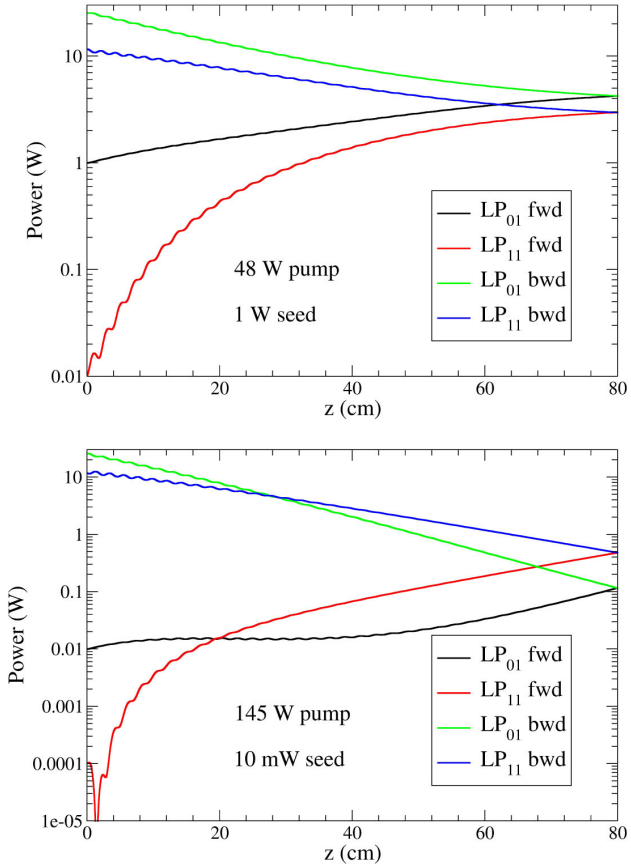

Fig. 10. Power distribution of forward- and backward-propagating signal modes along the length of the rod. Top: 1 W seed, 48 W pump power. Bottom: 10 mW seed, 145 W pump power.

in the experiments was not taken into account. Since the pump wavelength in the experiment gets closer to the optimum value with increasing pump power, i.e., for lower seeds, this effect counteracts the expected decrease in efficiency from reduced pump absorption. As a result, the experimental efficiency stays relatively constant around 44%, as evidenced in Fig. 5. It should be noted that both the experimental and numerical efficiency figures are system specific and can straightforwardly be improved without sacrificing total gain by optimizing the pump wavelength, increasing the rod length, and/or improving pump absorption by stronger core doping or an increased core/cladding area ratio.

To extract some physical insight from the model, Fig. 10 shows the power distribution of forward- and backward-propagating signal modes along the length of the rod. Two cases are illustrated, and both have a final HOM fraction of ∼0.31. In the first case, the seed power is 1 W, and the pump power is 48 W, whereas in the second case, the seed power is 10 mW, and the pump power is 145 W. The thermo-optic mode coupling between co-propagating LP_{01} and LP_{11} modes can be understood as scattering by thermo-optic long-period gratings arising from the beating patterns between the modes through the thermo-optic effect [5,6]. Now, in single-pass TMI models, it is established that the *static* grating set up by two co-propagating modes will have a phase relative to the modes that precludes power transfer into the HOM [6]; hence, single-pass TMI can

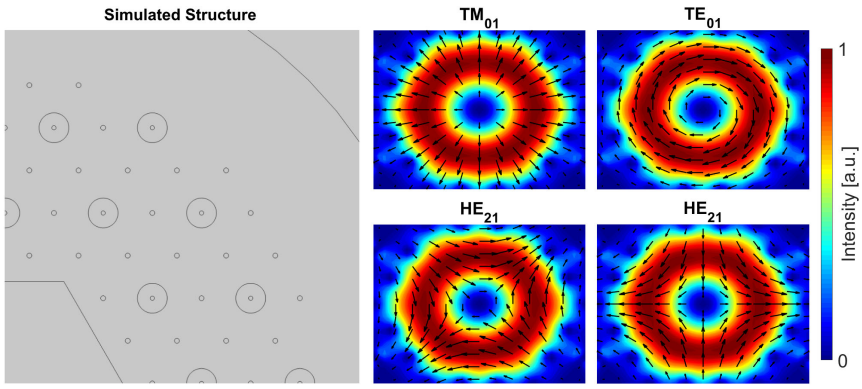

Fig. 11. Left: simulated quarter-structure of the aeroGAIN-ROD-PM85 amplifier. Small circles are airholes, larger circles are Ge-doped regions, and the hexagonal shape in the core region denotes the doped core. Right: intensity (color) and field (arrows) profiles of TE_{01}, HE_{21}, and TM_{01} modes in the core region.

be understood only in dynamic models. However, in a double-pass amplifier, efficient intermodal scattering may arise from the grating induced by beating between the two *counter-propagating* modes. The strongest grating is induced by the backward-propagating modes close to the input/output end, which carry the strongest signal power. Therefore, as clearly seen in Fig. 10, the power transfer between LP_{01} and LP_{11} happens mostly in the forward-propagating modes close to the input/output end. Subsequently, a suppression of the LP_{11} mode is observed, which is due to the lower core overlap of this mode and the resulting differential gain. As one can also see in the figure, the effect of a differential gain is much more severe when the total gain is higher, i.e., for low seed power. The ratio between LP_{11} and LP_{01} power at the reflection end is $\sim 3:4$ for the case of 1 W seed power, but $\sim 3:1$ for a 10 mW seed, although both solutions have $\sim 1:2$ ratio upon output. Further simulations (not shown) indicated that indeed the increase in threshold with decreasing seed power became less pronounced (although still present) when the V-parameter was increased to 3.0, and the differential gain between the modes thereby reduced. These findings suggest that HOM suppression by differential gain is particularly important in double-pass amplification due to the fact that most of the nonlinear mode coupling happens while the signal power is low, whereas in single-pass TMI, the strongest mode coupling appears close to the output where the signal power is high. Since the experimental rod most likely has better gain suppression than the step-index fiber described by the coupled-mode model, this could at least partly explain the higher SMD threshold observed in the experiments.

B. Origin of Polarization Rotation

A final outstanding issue is the origin of the nonlinear polarization rotations. The clear and consistent observation of this effect across the different optical setups used in this paper as well as [17] strongly suggests that the polarization change originates in the rod amplifier itself. A plausible model could be that linearly polarized light scattered into an LP_{11}-like HOM would undergo polarization rotation because the true eigenmodes of the waveguide are not LP modes but vector modes. Because the mode conversion happens along the fiber, the Faraday mirror will not necessarily undo it. On the other hand, in a step-index fiber model, the beat lengths of different vector modes in the LP_{11} multiplet are on the order of a kilometer for a core diameter of 85 μm, much too long for this explanation to be valid in a rod of 0.8 m length, even with two passes. The question is then whether the beat length of these vector modes is significantly shorter in the actual microstructured fiber.

To answer this question, finite-element simulations using the COMSOL Multiphysics tool were performed on a full structural model of the aeroGAIN-ROD-PM85 amplifier. Guided vector modes of TE_{01}, TM_{01}, and HE_{21} character were found, with core overlaps between 0.38 and 0.43 as mentioned above. The simulations did not consider any thermal load on the rod, but we expect the thermal lensing effects on guided-mode properties to be limited at the power levels reached in this work. Figure 11 shows the structural model and the mode profiles of the HOMs. The effective-index difference at a wavelength of 1.03 μm between TE_{01} and HE_{21} is $4.7 \cdot 10^{-7}$, and between HE_{21} and TM_{01}, it is $6.0 \cdot 10^{-7}$. The corresponding beat lengths are 2.2 and 1.7 m, respectively. Therefore, significant polarization rotation may occur in our propagation length of 1.6 m. In fact, almost full rotation seems possible, which could explain the complicated and non-monotonous behavior of discarded power versus pump power for some of the seed levels shown in Fig. 7.

Polarization rotation effects are usually not reported in single-pass TMI. We believe this is because the majority of the LP_{11} power seen on output is actually coupled into the LP_{11} multiplet close to the end of the amplifier in the single-pass case, due to the rapid exponential growth of HOM power with distance in this case. On the other hand, as discussed in the previous subsection, in the double-pass case, most intermodal scattering occurs early in the first pass of the amplifier, and so there is room for polarization rotation to take effect.

6. CONCLUSION

In conclusion, we have investigated an alternative setup for dual-pass amplification using a rod-type fiber. The main difference from our previous work consists of a polarization filtering

between the first and the second pass. This additional component decreases the global performance of the amplifier. The most important change is an unwanted reduction by a factor of 2.4 in the maximal signal output power for 300 mW input seed power (see Fig. 6). In line with our previous work, we find this maximum power to coincide with the TMI threshold. However, sweeping the seed power, we find that the TMI and SMD thresholds increase with decreasing seed power. At a seed power of 10 mW, we obtain 113 W output, corresponding to a gain of more than 40 dB. This is the highest value of gain reported for a rod-type amplifier module (to the best of our knowledge).

In addition, we report a logarithmic behavior between maximum gain and input seed power (Fig. 6), a mitigation of SMD (Fig. 7), and a "strong" static degradation below threshold for 100 mW input seed (Fig. 7). Each of these points is important for the future understanding of these phenomena. Simulations using a currently established model indicate that the threshold increase with seed power decreasing is due to an increased impact of differential gain, which seems particularly important in double-pass amplifiers because the strongest nonlinear mode coupling occurs on the input side where the signal power is low. Simulations of higher-order vector modes using an accurate finite-element tool show that the observed polarization rotations occurring in the double-pass setup may be explained by polarization rotation in the modes of the LP_{11} multiplet, since the vector modes have beat lengths on the order of 2 m among each other. At the same time, our consistent observation of the polarization rotation in different optical configurations makes it unlikely that the effect should originate in intensity-dependent deformations of components external to the rod amplifier.

From an application point of view, this source produce 100 W of 20 ps pulses at 1030 nm with a repetition rate of 20 MHz, nearly Gaussian beam, and a PER of 33 dB (limited by the output PBS). For perspective, such a double-pass setup might be used to directly amplify low-power fiber-based seed oscillators to ∼100 W output, and this could be of great interest for making compact chirped pulse amplification (CPA) sources with a reduced number of amplifier stages.

Funding. Teknologi og Produktion, Det Frie Forskningsråd (DFF-6111-00312).

Acknowledgment. J.-F. Lupi and J. Lægsgaard acknowledge financial support from the Danish Council for Independent Research-Technology and Production Sciences (FTP).

Disclosures. JFL, SLC: NKT Photonics (F); MMJ, MM: NKT Photonics (E); JL: NKT Photonics (C). The authors declare no conflicts of interest.

REFERENCES

1. D. J. Richardson, J. Nilsson, and W. A. Clarkson, "High power fiber lasers: current status and future perspectives," J. Opt. Soc. Am. B **27**, B63–B92 (2010).
2. C. Jauregui, J. Limpert, and A. Tünnermann, "High-power fibre lasers," Nat. Photonics **7**, 861 (2013).
3. M. N. Zervas and C. A. Codemard, "High power fiber lasers: a review," IEEE J. Sel. Top. Quantum Electron. **20**, 219–241 (2014).
4. T. Eidam, S. Hanf, E. Seise, T. V. Andersen, T. Gabler, C. Wirth, T. Schreiber, J. Limpert, and A. Tünnermann, "Femtosecond fiber CPA system emitting 830 W average output power," Opt. Lett. **35**, 94–96 (2010).
5. T. Eidam, C. Wirth, C. Jauregui, F. Stutzki, F. Jansen, H.-J. Otto, O. Schmidt, T. Schreiber, J. Limpert, and A. Tünnermann, "Experimental observations of the threshold-like onset of mode instabilities in high power fiber amplifiers," Opt. Express **19**, 13218–13224 (2011).
6. A. V. Smith and J. J. Smith, "Mode instability in high power fiber amplifiers," Opt. Express **19**, 10180–10192 (2011).
7. C. Jauregui, T. Eidam, J. Limpert, and A. Tünnermann, "Impact of modal interference on the beam quality of high-power fiber amplifiers," Opt. Express **19**, 3258–3271 (2011).
8. C. Jauregui, T. Eidam, H.-J. Otto, F. Stutzki, F. Jansen, J. Limpert, and A. Tünnermann, "Physical origin of mode instabilities in high-power fiber laser systems," Opt. Express **20**, 12912–12925 (2012).
9. K. R. Hansen, T. T. Alkeskjold, J. Broeng, and J. Lægsgaard, "Thermally induced mode coupling in rare-earth doped fiber amplifiers," Opt. Lett. **37**, 2382–2384 (2012).
10. K. R. Hansen, T. T. Alkeskjold, J. Broeng, and J. Lægsgaard, "Theoretical analysis of mode instability in high-power fiber amplifiers," Opt. Express **21**, 1944–1971 (2013).
11. B. G. Ward, "Modeling of transient modal instability in fiber amplifiers," Opt. Express **21**, 12053–12067 (2013).
12. L. Dong, "Stimulated thermal Rayleigh scattering in optical fibers," Opt. Express **21**, 2642–2656 (2013).
13. C. Jauregui, H.-J. Otto, F. Stutzki, J. Limpert, and A. Tünnermann, "Simplified modelling the mode instability threshold of high power fiber amplifiers in the presence of photodarkening," Opt. Express **23**, 20203–20218 (2015).
14. H.-J. Otto, N. Modsching, C. Jauregui, J. Limpert, and A. Tünnermann, "Impact of photodarkening on the mode instability threshold," Opt. Express **23**, 15265–15277 (2015).
15. J. Lægsgaard, "Static thermo-optic instability in double-pass fiber amplifiers," Opt. Express **24**, 13429–13443 (2016).
16. C. Stihler, H.-J. Otto, C. Jauregui, J. Limpert, and A. Tünnermann, "Experimental investigation of transverse mode instabilities in a double-pass yb-doped rod-type fiber amplifier," Proc. SPIE **10083**, 100830R (2017).
17. J.-F. Lupi, M. M. Johansen, M. Michieletto, and J. Lægsgaard, "Static and dynamic mode coupling in a double-pass rod-type fiber amplifier," Opt. Lett. **43**, 5535–5538 (2018).
18. Y. Zaouter, F. Guichard, L. Daniault, M. Hanna, F. Morin, C. Hönninger, E. Mottay, F. Druon, and P. Georges, "Femtosecond fiber chirped-and divided-pulse amplification system," Opt. Lett. **38**, 106–108 (2013).
19. R. Tao, X. Wang, and P. Zhou, "Comprehensive theoretical study of mode instability in high-power fiber lasers by employing a universal model and its implications," IEEE J. Sel. Top. Quantum Electron. **24**, 1–19 (2018).
20. C. Stihler, C. Jauregui, A. Tünnermann, and J. Limpert, "The impact of pump-power noise on transverse mode instabilities," Proc. SPIE **10897**, 1089703 (2019).
21. C. Stihler, C. Jauregui, A. Tünnermann, and J. Limpert, "Pump-power-noise influence on mode instabilities in high-power fiber laser systems," in *The European Conference on Lasers and Electro-Optics* (Optical Society of America, 2019), paper cj_4_6.
22. M. M. Johansen, M. Laurila, M. D. Maack, D. Noordegraaf, C. Jakobsen, T. T. Alkeskjold, and J. Lægsgaard, "Frequency resolved transverse mode instability in rod fiber amplifiers," Opt. Express **21**, 21847–21856 (2013).
23. T. T. Alkeskjold, M. Laurila, L. Scolari, and J. Broeng, "Single-mode ytterbium-doped large-mode-area photonic bandgap rod fiber amplifier," Opt. Express **19**, 7398–7409 (2011).
24. A. V. Smith and J. J. Smith, "Increasing mode instability thresholds of fiber amplifiers by gain saturation," Opt. Express **21**, 15168–15182 (2013).
25. K. R. Hansen and J. Lægsgaard, "Impact of gain saturation on the mode instability threshold in high-power fiber amplifiers," Opt. Express **22**, 11267–11278 (2014).